Nuclear Instruments and Methods in Physics Research A 793 (2015) 101–107

Contents lists available at ScienceDirect

Nuclear Instruments and Methods in Physics Research A

journal homepage: www.elsevier.com/locate/nima

Neutron response function characterization of ^{4}He scintillation detectors

Ryan P. Kelley [a,*], Lucas M. Rolison [a], Jason M. Lewis [a], David Murer [b], Thomas N. Massey [c], Andreas Enqvist [a], Kelly A. Jordan [a]

[a] University of Florida, Nuclear Engineering Program, Gainesville, FL 32611-6400, United States
[b] Arktis Radiation Detectors Ltd., Räffelstrasse 11, 8045 Zürich, Switzerland
[c] Ohio University, Institute of Nuclear and Particle Physics, Athens, OH 45701, United States

ARTICLE INFO

Article history:
Received 8 September 2014
Received in revised form
9 January 2015
Accepted 7 April 2015
Available online 15 April 2015

Keywords:
Neutron detection
Scintillators
^{4}He
Time-of-flight

ABSTRACT

Time-of-flight measurements were conducted to characterize the neutron energy response of pressurized ^{4}He fast neutron scintillation detectors for the first time, using the Van de Graaff generator at Ohio University. The time-of-flight spectra and pulse height distributions were measured. This data was used to determine the light output response function, which was found to be linear at energies below 3.5 MeV. The intrinsic efficiency of the detector as a function of incident energy was also calculated: the average efficiency up to 10 MeV was 3.1%, with a maximum efficiency of 6.6% at 1.05 MeV. These results will enable development of neutron spectrum unfolding algorithms for neutron spectroscopy applications with these detectors.

1. Introduction

This paper describes the characterization of ^{4}He fast neutron scintillation detectors and the determination of the detector response matrix using the Van de Graaff generator at Ohio University (OU). High-accuracy time-of-flight (TOF) measurements were achieved by calculating the difference between the timestamp of each neutron event in the ^{4}He detector and the start time of the generator pulse. With a known distance of 10 m between the target and the detector, the TOF was converted to determine the incident neutron energy. Comparing the incident energy of each neutron with the resulting light output measured by the detector enabled a series of detector parameters to be evaluated, including the light output distributions as a function of neutron energy, the energy-dependent detector efficiency up to 10 MeV, and the detector response matrix, which will enable the development of unfolding algorithms for neutron spectroscopy applications.

The ^{4}He detector, developed by Arktis Radiation Detectors Ltd., can be implemented in a wide range of applications. Previous work has shown that their energy discrimination abilities can be used to measure the plutonium content in mixed oxide fuel by discriminating between neutrons produced by spontaneous fission and neutrons from the (α,n) reaction with oxygen [1]. Other work has demonstrated that, by irradiating a sample of natural uranium using a (d,d) neutron generator to simulate the active interrogation of cargo containers, ^{4}He detectors provide an unambiguous indication of the presence of fissile material [2], which has direct applications to the detection of hidden shielded nuclear material. The methods developed in these studies, however, are limited to interpretations of the photon output from the detector, since the relationship between neutron energy and light output was not previously known.

1.1. ^{4}He detectors

Thermal neutron detectors such as ^{3}He proportional counters have traditionally dominated the world of neutron detection because of their low cost, robust design, and high detection efficiencies. Pressurized ^{4}He scintillation detectors provide performance advantages including background rejection and retention of neutron energy information. Similarly, they offer a potential solution to the worldwide ^{3}He supply shortage, caused by the simultaneous reduction in nuclear weapon inventories (the primary source of production of ^{3}He gas) and the increasing demand for ^{3}He neutron detectors in border security markets [3].

The operation of ^{3}He counters is based on the absorption of thermal neutrons in the detector gas. Detectors filled with ^{4}He, on the other hand, rely on its high cross-section for elastic scattering with fast neutrons. These detectors are simple in design, as illustrated in Fig. 1, and are manufactured in several sizes. The model used in this experiment had an active volume length of 20 cm, with an inner diameter of 4.4 cm, giving a total active volume of 304 cm^{3}. The key

* Corresponding author.

http://dx.doi.org/10.1016/j.nima.2015.04.011
0168-9002/

components include the active volume, filled with 150 bar of ^{4}He gas, and photomultiplier tubes (PMTs) mounted at either end of the active volume [4]. The PMTs operate with a supply voltage between 1400 and 1750 Vdc, and have a quantum efficiency of 27% at 420 nm [5]. The detector body is made of stainless steel.

A neutron scattering interaction within the detector volume transfers a portion of the neutron's kinetic energy to a ^{4}He nucleus, as a function of the scattering angle. The neutron is not absorbed in this process, but rather continues to travel in a new direction and with reduced kinetic energy. This transfer of energy strips electrons from the target ^{4}He nucleus, which then moves through the gas as a recoil alpha particle. This recoil alpha interacts with other helium atoms along its path through excitation or ionization.

These ionizations and excitations produce helium singlet and triplet excimer states. The decay of these excimers to the ground state produces scintillation photons, which are counted by the PMTs at either end of the tube. Using an AmBe neutron source, previous TOF experiments have shown that the number of photons produced and counted by the PMTs is proportional to the incident neutron energy [6].

Due to differences in the rate of decay of the singlet and triplet excimer states, each scintillation signal recorded by the PMTs can be separated in time into two components: a slow and a fast component. The fast component consists of a sharp light pulse that exists on the order of nanoseconds, while the slow component consists of multiple shorter pulses that are stretched over about four microseconds. Together, these two components make up the resulting raw signal trace, as shown in Fig. 2.

The ^{4}He data acquisition (DAQ) module has a sampling rate of 1 Gb/s at 10-bit resolution, with 16 channels. Field programmable gate arrays (FPGAs) within the DAQ search for coincident signals within 32 ns from the PMTs mounted on either side of a given detector. When coincidence between PMTs is verified, the event is read out from the DAQ to the control computer for storage. The event is discarded as PMT noise if there is no coincidence.

These ^{4}He detectors are nearly insensitive to gamma rays, due to the low electron density of the gas. Contrary to neutrons that interact with the nucleus of the atom, gamma rays interact with the atom's orbiting electrons. Helium's low atomic number ($Z=2$) results in a low electron density, which reduces the probability of gamma interaction. Additionally, gamma interactions in the active volume produce recoil electrons, and due to the low density of the gas even at high tube pressures, the rate of energy deposition by bremsstrahlung interactions will be low. The electron will travel farther while slowing down and will be more likely to hit a wall before depositing all of its energy. Gamma rays also have a lower light yield in gaseous helium scintillation when compared to neutron interactions, contrary to liquid scintillators.

The combined effects of lower energy deposition and lower light yield of gamma ray interactions in the helium gas result in the integrated slow component of a gamma event being up to 8 times smaller than that of a neutron event. This is illustrated in Fig. 3, which shows the signal trace from both a neutron event and a gamma event for comparison. By comparing the slow and the fast component of each event pulse shape discrimination (PSD) can be performed [6]. This was illustrated by using a ^{4}He detector to separately measure a ^{252}Cf neutron/gamma source (gray) and a ^{60}Co gamma source (white). Plotting the integrated slow component against the integrated fast component for each event gives the plot shown in Fig. 4, which shows the separation between the two types of particle interactions in the detector. The black diagonal line illustrates the PSD calibration line. Events landing above the line are retained as neutrons, while events below the line are discarded as gammas. Fig. 4 shows that some of the ^{60}Co gamma events will fall above the calibration line, and will be erroneously classified as neutrons, however this fraction was calculated to be only 1% of the total number of measured gamma events.

In addition to being useful for PSD, the amount of light detected in the slow component of a neutron event has been shown to be correlated with neutron energy, as demonstrated in previous AmBe TOF experiments [6]. The integrated slow component was therefore

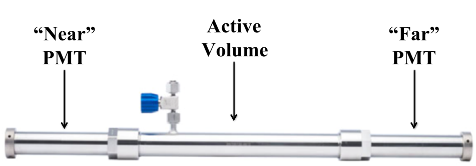

Fig. 1. The ^{4}He detector.

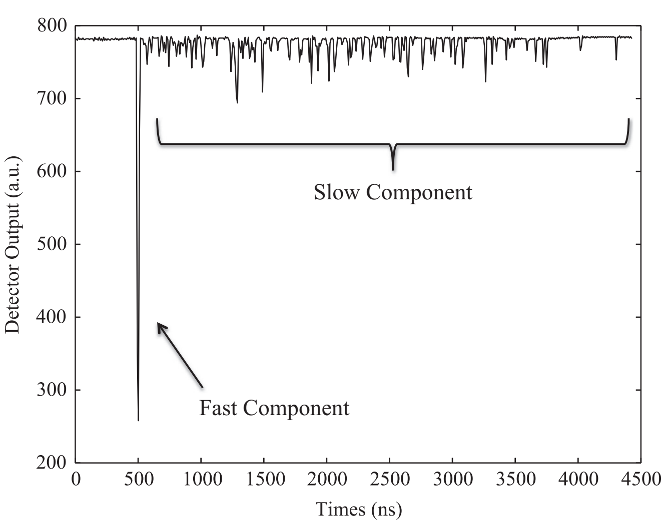

Fig. 2. ^{4}He detector output for a single neutron event, highlighting the slow and fast components.

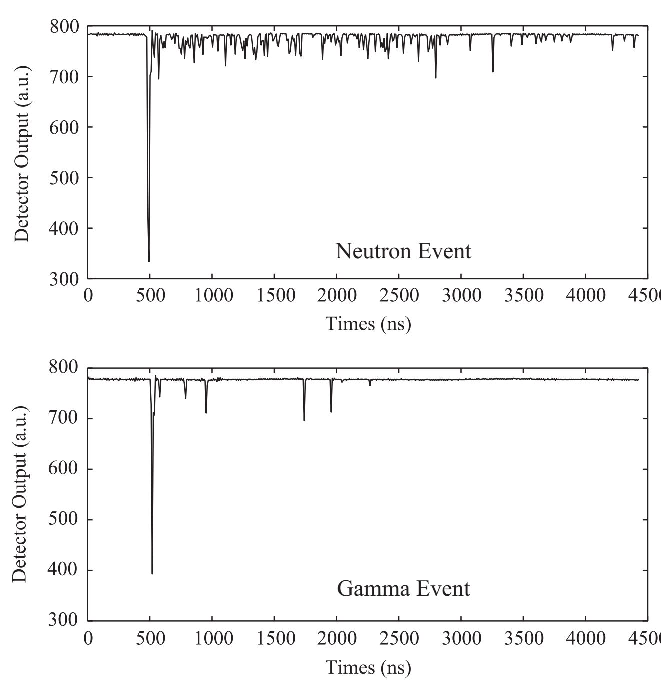

Fig. 3. ^{4}He detector output for a neutron event (top) and a gamma event (bottom). The fast components are comparable. The neutron slow component is much stronger than the gamma slow component, which forms the basis for the PSD algorithm.

used as the basis for measuring the resulting pulse height from each neutron event for the analysis of the experimental data.

The effects of aging on the pulse shape is a concern with scintillators, since the progression of time causes changes in the signal over long periods of time. In these ^{4}He detectors, an internal purification system is installed that prevents degradation of the scintillation pulse. During the time span that test detectors were monitored (3 years), no degradation of the scintillation pulse was observed. From a stimulated aging test, it is estimated that the life time of the detectors exceeds 10 years [7].

2. Experimental methods

A method for characterizing a neutron detector was detailed in previous literature by Kornilov et al., who showed that detector parameters such as intrinsic efficiency and the light output response function could be determined by using a ^{252}Cf source and TOF measurements with liquid scintillators [8]. Similarly, the work of Enqvist et al. built upon this method by characterizing a collection of liquid scintillators using the Van de Graaff generator at the Edwards Accelerator Facility at Ohio University [9]. This research uses the methods of analysis laid out in these previous works to conduct a characterization of ^{4}He scintillation detectors.

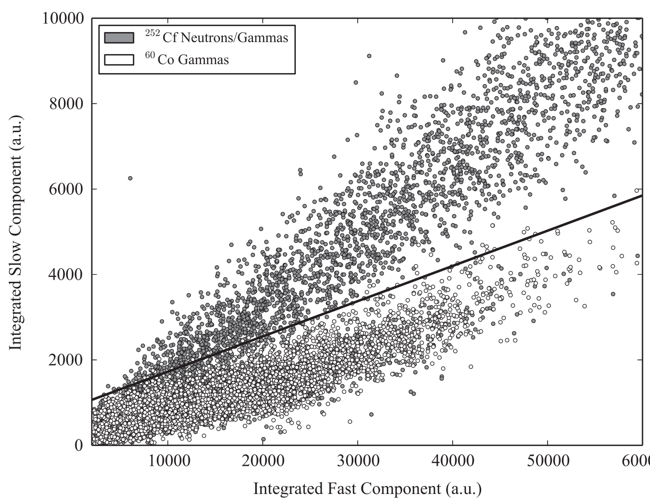

Fig. 4. The integrated slow component is plotted against the integrated fast component for each event in the detector. Since the slow component of a neutron event is up to eight times stronger than that of a gamma event, there is a separation between the particle types that is exploited for pulse shape discrimination.

The Edwards Accelerator facility provided an ideal environment for investigation into the neutron energy response of ^{4}He detectors. Their Van de Graaff generator produces a pulsed beam of protons, deuterons, or heavy ions that are accelerated onto a variety of targets, including ^{10}B, ^{27}Al, or carbon. Monoenergetic neutrons can be produced, as can a continuous spectrum of neutron energies. Conducting measurements in an 30 m underground tunnel, covered by 3 m of earth, reduced interference from cosmic rays and other sources of background radiation.

The orientation of the Edwards Accelerator Facility offers particle flight paths at various angles from the Van de Graaff generator, enabling the irradiation of a wide range of experimental configurations. For this experiment, 7.44 MeV deuterons were accelerated onto a ^{27}Al target, producing a neutron beam with a continuous spectrum of energies from a few hundred keV to over 10 MeV [10]. Neutrons were produced at a rate of 10^9 neutrons/Sr/s. A concrete collimator with a 10 cm diameter was used to confine the target's neutron flux into a beam that was directed down the 30 m tunnel, where the detectors were positioned (Fig. 5).

The distance from the aluminum target to the ^{4}He detectors was 10 m, which was close enough to the ^{27}Al target so that the neutron beam remained collimated, minimizing interference from neutrons scattered off the tunnel wall. Interference from neutrons scattering off the tunnel wall is a concern since these neutrons would interact in the detector with an incident energy different from the energy that would be calculated by the TOF method, and would be improperly correlated with detector light output. Fig. 6 shows the position of the detectors in the beam tunnel, behind the collimator wall.

The neutron beam was pulsed every 1600 ns (625 kHz) in order to allow time for the slowest neutrons from each pulse to reach the detector before the next pulse. The Van de Graaff generator is equipped with a beam swinger arm, which uses magnets to guide the beam to the target at an angle perpendicular to the original beam path. The swinger arm can be rotated around the target at any angle from -4 to 180°, thereby changing the angle between the deuteron beam and the detectors in the tunnel. For this research, the arm was positioned at 120°. This decision was based on previous work, which showed that smaller angles resulted in significant self-shielding of the thick aluminum target [10].

For each pulse of the generator beam, the passage of deuterons through the accelerator toward the aluminum target produced an electronic trigger signal that was routed to one channel of the ^{4}He

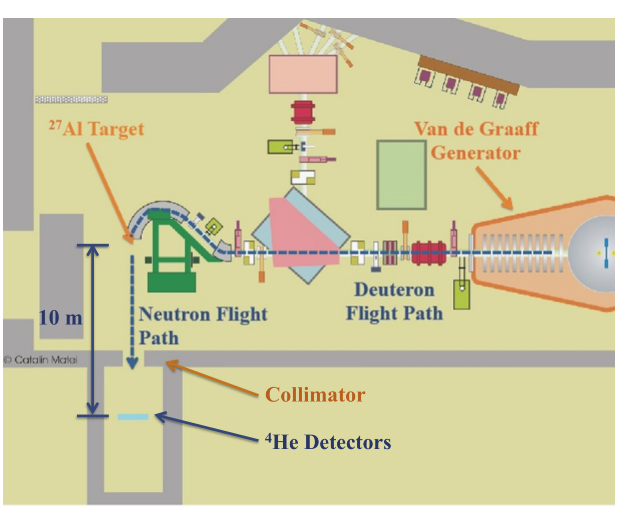

Fig. 5. The high-energy area of the Edwards Accelerator Facility at Ohio University.

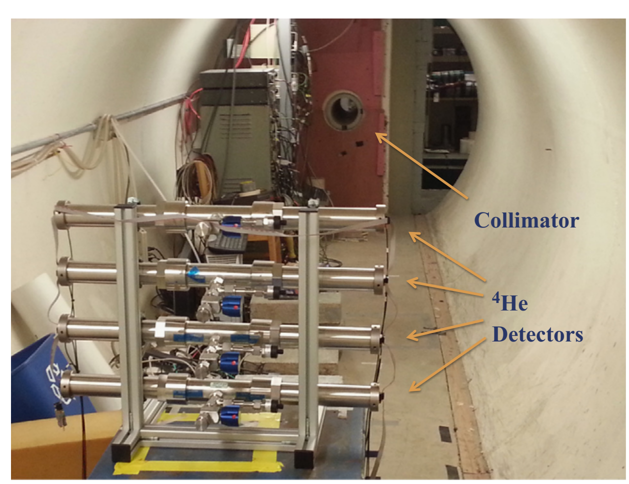

Fig. 6. Measurement setup showing the pulsed neutron beam collimator as seen from the ^{4}He detectors.

data acquisition module (DAQ). The DAQ used this trigger as a coincidence "start" signal for recording events from the detectors. Without a preceding signal from the generator, in other words, events in the detectors would not be recorded.

Fig. 7 is a two-dimensional histogram of the pulse height versus particle flight time. The pulse height bins are 2 units wide (arbitrary units of detector output, as read from the DAQ module); time bins are 5 ns wide. An increasing particle flight time (corresponding to decreasing incident neutron energy) results in decreasing light output, illustrating the correlation between particle TOF and detector response. This relationship was more thoroughly investigated by converting the TOF spectrum to the measured neutron energy spectrum.

Extracting only the particle flight time information from Fig. 7 yields the measured TOF spectrum shown in Fig. 8, which shows 1 ns time bins. The beam pick-off signal that marks the start of each pulse is not triggered from deuteron arrival at the aluminum target, but rather from a fixed position earlier in the deuteron's flight path through the accelerator. Combined with delays from propagation of the signal through cables of various lengths, the result is a constant time delay of the start trigger, which must be accounted for when performing TOF calculations. This was accomplished by alignment of the gamma-flash in the TOF spectrum.

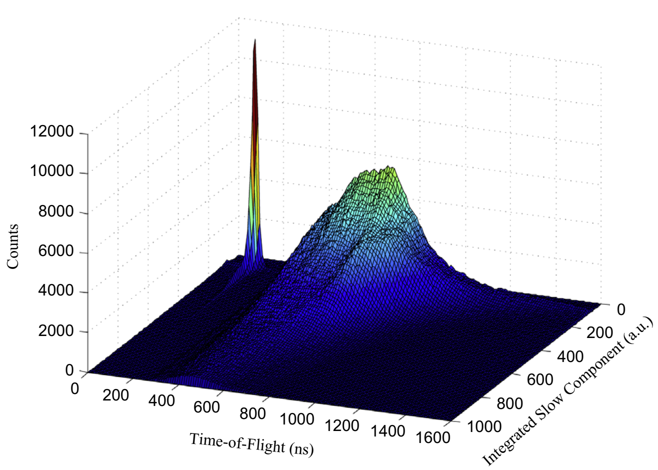

Fig. 7. The measured ^{4}He light response as a function of particle time-of-flight (TOF).

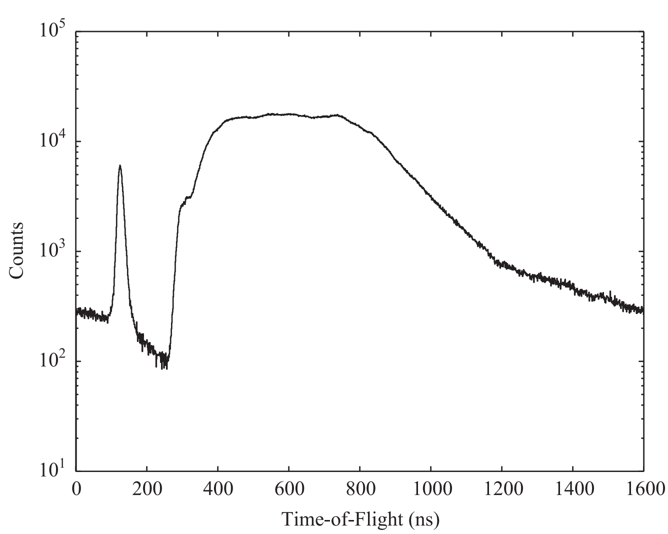

Fig. 8. The TOF spectrum. The data shown represents 9.5×10^{6} events, divided into 1 ns wide bins.

This gamma-flash is caused by gamma rays produced from the impact of the deuteron beam on the ^{27}Al target, and will be the first signal to reach the detector. Traveling at the speed of light from the target over the known distance of 10 m to the detectors, these gammas should be observed at 33 ns on the TOF spectrum. Any time deviation of this gamma peak in the raw TOF spectrum is due to associated delays, and can be used to apply a constant corrective shift to the TOF spectrum. After applying this correction, the time it took each neutron to travel from the ^{27}Al target to the ^{4}He detector could be determined, and, using the flight distance, was then converted to that neutron's incident energy as it interacted in the detector. These energies are compiled in the histogram shown in Fig. 9.

When applied to the measurements conducted at OU, the PSD algorithm retained 0.2% of gamma events as neutrons, which was calculated by comparing the area under the gamma flash from the measurements before and after the application of the PSD algorithm. Since the gamma flash is known to be composed of gammas events, the area under this peak after the application of the PSD algorithm should be minimized. Any events that are retained in this gamma flash represent gammas that were erroneously classified by the PSD algorithm as neutrons. This value represents only the gamma ray retention rate: the fraction of gamma rays interacting in the detector that are classified as neutrons by the PSD algorithm. It fails to account for the fact that the gamma interaction rate in the detector is already reduced by the inherently low gamma ray interaction efficiency of a ^{4}He detector, as described in Section 1.1.

By solid body elastic scattering kinematics, a neutron will transfer a maximum of 64% of its incident energy to a ^{4}He nucleus in the detector volume [11]. This relationship is given by: ($E_R = 2A/(1+A)^2(1-\cos\theta)E_n$, where A is the atomic mass of the helium atom, E_n is the incident neutron energy, and E_R is the energy lost by the neutron in a scattering interaction that changes its direction of travel by an angle θ.

For a given neutron energy a 64% energy transfer will correspond to the maximum measured light output for that energy. The result should be a sharp edge at the upper range of the output distribution, similar to that illustrated in Fig. 10. This distribution was generated by using MCNPX-PoliMi [12] to record the energy deposited in a simulated ^{4}He detector by monoenergetic 2.45 MeV neutrons.

MCNPX-PoliMi was also used to simulate the number of multiple-scatter events that can be expected. These events were rare: only 4% of simulated neutrons experienced more than one

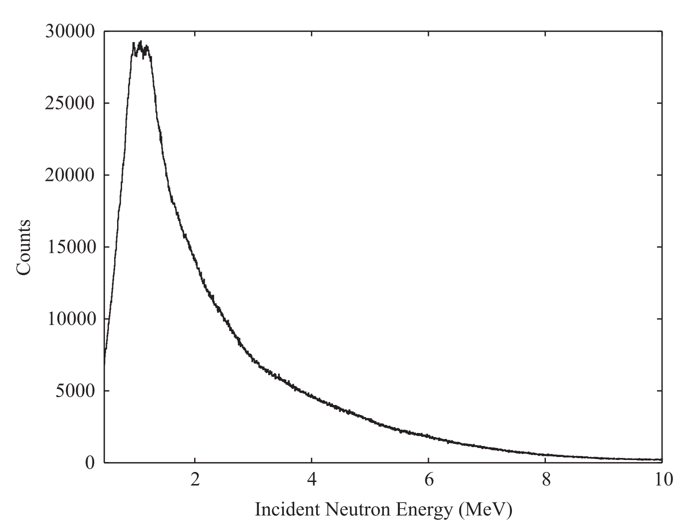

Fig. 9. The incident neutron energy spectrum, as measured by TOF.

scattering event. Due to this low probability of occurrence, the effect of possible double-scatterings was not corrected for in this analysis.

Additionally, the low probability of multiple scatters for a neutron is beneficial with respect to the relationship between deposited energy and light output. In liquid scintillators, for example, it is common for the same neutron to undergo multiple scattering interactions, and with different atoms (carbon or hydrogen). Each material has a different relationship between the energy deposited and the light produced, making unfolding complicated.

3. Results and discussion

3.1. Light output distributions

Fig. 11 shows a collection of light output distributions for several incident neutron energies, as measured by the ^{4}He detectors at the Edwards Facility during these TOF measurements. Only the light output distributions for incident neutron energies of

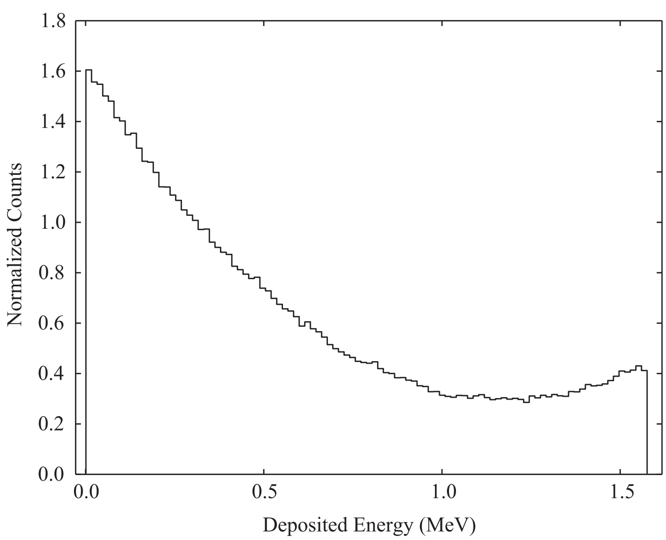

Fig. 10. MCNPX-PoliMi data from 2.45 MeV neutrons measured by a ^{4}He detector.

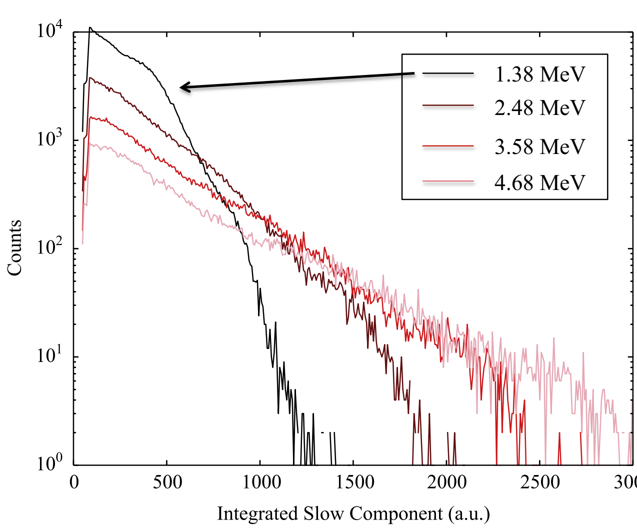

Fig. 11. Measured light output distributions for neutron energies from 1.38 MeV to 4.68 MeV, in 1.10 MeV increments. Actual bin sizes for these distributions are 0.11 MeV.

1.38, 2.48, 3.58, and 4.68 MeV are plotted, for clarity. The shape of these distributions lacks the sharp upper edge shown in Fig. 10 due to the distribution being blurred by the system's energy resolution. The number of neutrons measured in each energy group varies based on the neutron flux from the aluminum target, as well as the changes in the elastic scattering cross-section of ^{4}He as a function of neutron energy.

Each of these light output distributions was then analyzed according to the process used by Kornilov et al. [8], whereby the individual distributions were smoothed using a nine-window moving average in order to minimize statistical instabilities. Then, the derivative of this smoothed distribution was calculated. Kornilov et al. described how the energy resolution of a detector could be measured by fitting a Gaussian curve to this derivative's upper edge, however the broadening observed in Fig. 11 was too wide, and did not allow a quantitative estimation of the detector's energy resolution to be obtained.

3.2. Neutron light output response function

The ^{4}He response matrix obtained from the OU measurements is shown in Fig. 12, which is a two-dimensional histogram of the pulse height versus incident neutron energy. Each of the columns of the response matrix represents the response function for an incident neutron energy, up to 5.5 MeV. The rows correspond to various integrated slow component bins, up to 1000 units (arbitrary units of detector output, as read from the DAQ module). Again, the integrated slow component of each event is used as the basis for the pulse height. Pulse height bins are 2 units wide; energy bins are 0.11 MeV wide.

Fig. 13 shows the ^{4}He detector measured light output response function. A linear approximation can be used below about 3.5 MeV to represent the relationship between incident neutron energy and measured light output ($R^2 = 0.95737$). This disagrees with previous work by Esterling and Lipman [13], which showed that their helium gas scintillator has a linear relationship between light output and energy up to their maximum measured energy of 5.5 MeV.

The investigation of individual event traces, such as the trace shown in Fig. 14, shows that this is due to the saturation of the dynamic range of the DAQ module. These high-energy events saturate the maximum pulse height which can be recorded with the DAQ, truncating the peak of the slow component pulse. This results in a reduced slow component light output being recorded for

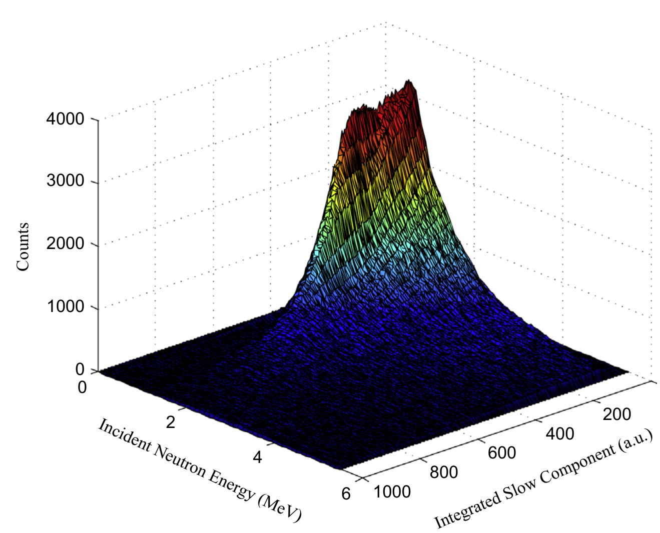

Fig. 12. The measured ^{4}He response matrix.

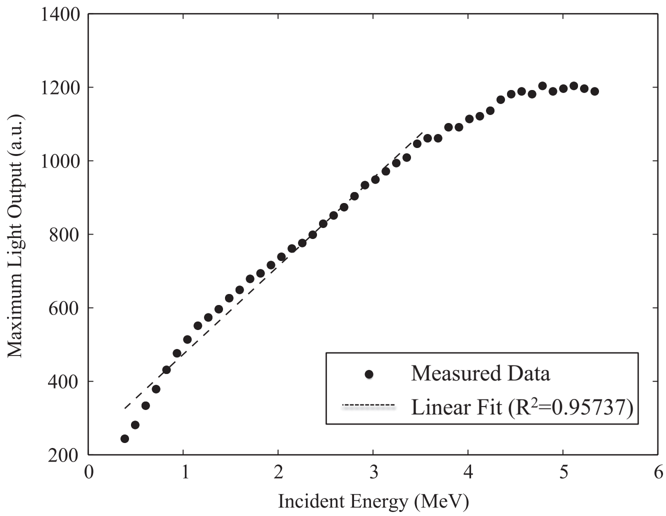

Fig. 13. The light function for a ^{4}He gas scintillation detector.

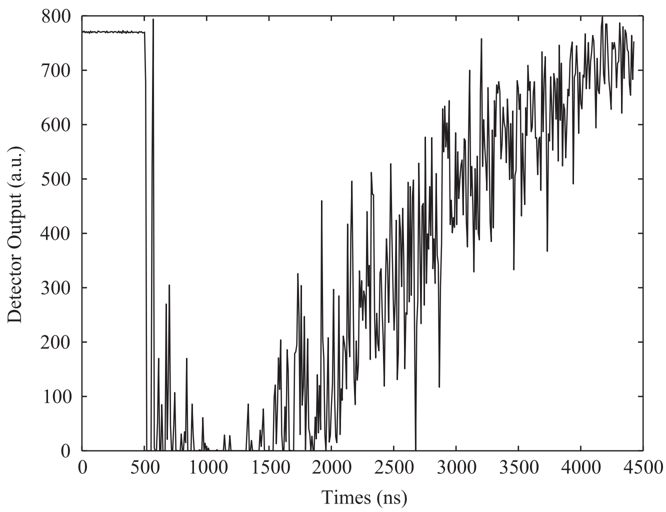

Fig. 14. Detector output for a neutron event, illustrating saturation of the slow component.

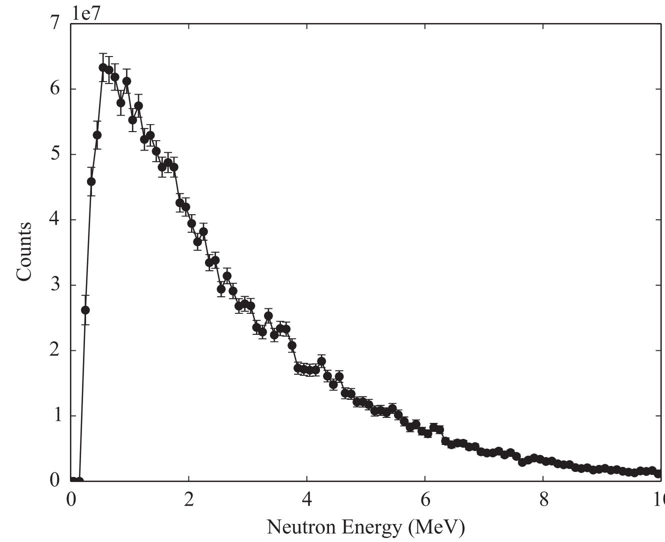

Fig. 15. Experimental neutron flux from the ^{27}Al(d,n) reaction. This data was used to calculate the intrinsic efficiency for a ^{4}He detector.

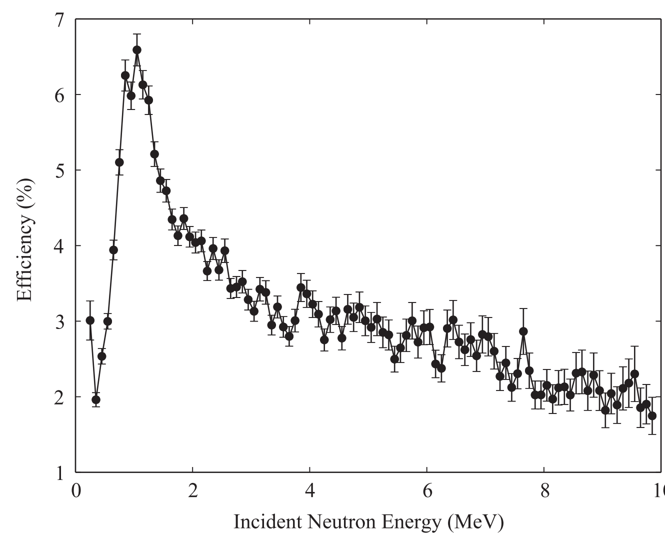

Fig. 16. ^{4}He detector interaction efficiency as a function of incident neutron energy.

the event than was actually seen by the PMTs. A point is therefore reached where higher energy events cease to result in a higher light output, thus resulting in the flattening of the curve in Fig. 13.

3.3. *Energy-dependent efficiency*

Previous work has measured the experimental flux from the ^{27}Al(d,n) reaction used in these measurements for the purpose of neutron detector calibration (Fig. 15) [10]. This emission spectrum was compared to the ^{4}He-detected spectrum (Fig. 9). Calculating the ratio between the number of neutrons detected and emitted in each energy group provides an energy-dependent efficiency relationship, as shown in Fig. 16. The average measured efficiency up to neutron energies of 10 MeV was 3.1%. The maximum efficiency was 6.6% at 1.05 MeV. GEANT and MCNPX efficiency analyses estimated a peak efficiency of 9.0% at 1.00 MeV, compared to the 6.6% measured by this work [6]. The difference in these efficiencies is due to the scintillation properties of the gas, as well as the light propagation properties of the tube, which cannot be entirely predicted by simulation.

4. Conclusions

Fast neutron ^{4}He scintillation detectors have multiple performance advantages, including neutron background rejection, gamma ray rejection, and the preservation of neutron energy information. Due to a lack of energy response information, their applications up to this point have been limited to an interpretation of the detected light output spectrum. This research characterized ^{4}He detectors and measured the neutron energy response function.

The Van de Graaff generator at Ohio University's Edwards Accelerator Facility was used to conduct TOF measurements. Neutrons with energies up to 10 MeV were generated by the ^{27}Al (d,n) reaction, using 7.44 MeV deuterons. The incident neutron energy and the resulting light output for each event were recorded and analyzed.

This experimental data was used to measure the intrinsic efficiency of the detectors as a function of incident neutron energy. The average efficiency over the range up to 10 Mev was found to be 3.1%. Previous studies had only approximated this energy-dependent efficiency relationship using GEANT and MCNPX simulations. These experimental measurements will allow for parametric studies on the implementation of ^{4}He detectors for cargo-scanning and oil/gas exploration.

The neutron response matrix and response function were also determined, and the response function was shown to be linear below 3.5 MeV. This linear relationship between light output and neutron energy is beneficial for future spectral unfolding efforts. The neutron response matrix shows the relationships between neutron energy and resulting light output, and therefore gives a probabilistic understanding of which neutron energies are most likely to produce a given light output. The neutron energy spectrum can then be unfolded by iteratively solving for an energy spectrum solution that best reproduces a given ^{4}He detector light distribution, similar to the methods used to unfold neutron spectra from Bonner sphere measurements [14]. The results of this work will therefore enable the use of ^{4}He detectors for the unfolding of neutron spectra, in order to produce a neutron spectrometer with gamma insensitivity.

Acknowledgments

The authors would like to thank the personnel at the Ohio University Edwards Accelerator Facility, especially Don Carter for electronics support and Devon Jacobs for accelerator setup. Their assistance made this work possible. This work was funded by an Nuclear Regulatory Commission Graduate Fellowship.

References

[1] D. Murer, R. Chandra, G. Davatz, H. Friederich, U. Gendotti, A. Howard, R. Lanza, P. Peerani, A. Tomanin, IEEE Nuclear Science Symposium Conference Record (2011) 4858.
[2] J.M. Lewis, R.P. Kelley, D. Murer, K.A. Jordan, Applied Physics Letters 105 (2014).
[3] R.T. Kouzes, J.H. Ely, L.E. Erikson, W.J. Kernan, A.T. Lintereur, E.R. Siciliano, D. L. Stephens, D.C. Stromswold, R.M. vanGinhoven, M.L. Woodring, Nuclear Instruments and Methods in Physics Research Section A 623 (2010) 1035.
[4] Product Catalog, Arktis Radiation Detectors Ltd. Zurich, Switzerland.
[5] Hamamatsu Photonics Technical Data Sheet, R580.
[6] R. Chandra, G. Davatz, H. Friederich, U. Gendotti, D. Murer, Journal of Instrumentation 7 (03) (2012) C03035.
[7] Personal communication, Arktis Radiation Detectors Ltd., December 2014.
[8] N.V. Kornilov, I. Fabry, S. Oberstedt, F.-J. Hambsch, Nuclear Instruments and Methods in Physics Research Section A 599 (2009) 226.
[9] A. Enqvist, C.C. Lawrence, B.M. Wieger, S.A. Pozzi, T.N. Massey, Nuclear Instruments and Methods in Physics Research Section A 715 (2013) 79.
[10] T.N. Massey, S. Al-Quraishi, C.E. Brient, J.F. Guillemette, S.M. Grimes, D. Jacobs, J.E. O'Donnell, J. Oldendick, R. Wheeler, Nuclear Science and Engineering (1998).
[11] J.L. Lewis, D. Raetz, D. Murer, K.A. Jordan, Analysis for in-situ fission rate measurements using ^{4}He gas scintillation detectors, in: IEEE, 2013.
[12] S.A. Pozzi, S.D. Clarke, W. Walsh, E.C. Miller, J. Dolan, M. Flaska, B.M. Wieger, A. Enqvist, E. Padovani, J.K. Mattingly, D. Chichester, P. Peerani, Nuclear Instruments and Methods in Physics Research Section A 694 (2012) 119.
[13] R.J. Esterling, N.H. Lipman, Review of Scientific Instruments 36 (1965) 492.
[14] D.W. Freeman, R. Edwards, A.E. Bolon, Nuclear Instruments and Methods in Physics Research Section A 425 (3) (1999) 549.